Journal of Water Process Engineering 77 (2025) 108508

Contents lists available at ScienceDirect

Journal of Water Process Engineering

journal homepage: www.elsevier.com/locate/jwpe

Exploratory data analysis and economic feasibility on the scale-up of an industrial wastewater treatment using a green nanocatalyst in heterogeneous photocatalysis system

Leandro Rodrigues Oviedo [a], Sthéfany Nunes Loureiro [a], Lissandro Dorneles Dalla Nora [a], William Leonardo da Silva [a,*]

[a] Applied Nanomaterials Research Group (GPNAp), Nanoscience Graduate Program, Franciscan University (UFN), Santa Maria, RS, Brazil

ARTICLE INFO

Editor: Guangming Jiang

Keywords:
Advanced oxidation processes
Data analysis
Economic feasibility
Green nanocatalysts
Wastewater treatment

ABSTRACT

The expansion of an industrial wastewater treatment system, while essential for sustainability and environmental compliance, is a complex project that presents significant challenges, both in exploratory data analysis and in assessing economic feasibility, involving gaps in data quality and availability, wastewater complexity and variability, projected operating costs, and the availability of financing and incentives. In this context, the present work aims to evaluate the economic feasibility and exploratory data analysis (EDA) of the production of a green supported nanocatalyst (nSOD@CuO-NPs) composed of a catalytic matrix of nanozeolite sodalite (nSOD) obtained from aluminum sludge and rice husk waste, while copper oxide nanoparticles (CuO-NPs) prepared by the green synthesis method from green tea (*Camellia sinensis*) serve as the photoactive phase for the degradation of a binary dye mixture of crystal violet and methylene blue (CV: MB) at an industrial scale. Heterogeneous photocatalysis was carried out under visible radiation ([CV:MB] = 70 and 135 mg L^{-1} | [nSOD@CuO-NPs] = 0.5–1.5 g L^{-1} | pH 4–10) for 240 min by the Central Composite Rotatable Design (CCRD). Net Present Value (NPV), Internal Return Rate (IRR), Cost-Benefit ratio (B/C), and Discounted Payback Period (DPP) were used to evaluate the economic feasibility of nSOD@CuO-NPs production (15–45 kg day^{-1}). The economic analysis revealed that all systems were economically viable, with IRR greater than the interest rate (i = 12 %). System 3 was the most reliable system (NVP = US$ 2,845,471.11, B/C = 2.50, IRR = 59.7 %, DPP = 2 years).

1. Introduction

Wastewater contamination by organic pollutants is one of the greatest global challenges, with an estimated 380 trillion liters improperly disposed of each year, raising serious environmental concerns [1]. Among the pollutants present, synthetic dyes (e.g., crystal violet – CV and methylene blue – MB) are widely used in the textile, pharmaceutical, and laboratory industries for fabric dyeing, biological staining, and even medical treatments [2].

Crystal violet (CV) and methylene blue (MB) dyes are highly persistent and toxic to the environment, causing deleterious effects on aquatic life, such as impairment of metabolism and reproduction of aquatic animals [3]. These contaminants can reduce light penetration in water, disbalancing photosynthesis in aquatic ecosystems [4]. Additionally, studies reported that crystal violet has carcinogenic and mutagenic potential, further exacerbating its ecological and public health risks [5].

In this sense, efficient technologies such as Advanced Oxidation Processes (e.g., heterogeneous photocatalysis, photo-Fenton process, ozonation) are required to degrade these pollutants efficiently from wastewater [6]. Heterogenous photocatalysis has been promising in removing organic pollutants (e.g., synthetic dyes, pharmaceuticals, pesticides) since it uses nanomaterials (heterogeneous supported nanocatalysts) that are activated by UV/visible radiation that generates oxygen radical species (•OH, $\bullet O_2^-$ from dissolved oxygen and water molecule) thus providing the mineralization of these organic contaminants [7,8]. In addition, heterogeneous photocatalysis is an eco-friendly and versatile process, being used under sunlight irradiation [9].

Numerous supported nanocatalysts have been used in photocatalysis, in special copper oxide nanoparticles supported onto nanozeolites (nZ@CuO-NPs) due to their good thermal/physiochemical stability, narrow band gap energy (1.20–2.22 eV), surface acidity, and

* Corresponding author.
E-mail address: williamleonardo_silva@hotmail.com (W.L. da Silva).

https://doi.org/10.1016/j.jwpe.2025.108508
Received 3 June 2025; Received in revised form 29 July 2025; Accepted 11 August 2025
Available online 16 August 2025

textural properties [10,11]. Additionally, CuO-NPs can be prepared by green synthesis at low to moderate temperatures using plant extracts as reducing agents [12]. In addition, nanozeolites are microporous crystalline aluminosilicates on a nanometer scale, recognized for their intrinsic and specific properties, such as a high surface area with improved diffusion and mass transport rates, better accessibility to active sites for target chemical species, and modified optical and electronic properties [13]. By these reasons, nanozeolites can be characterized as suitable catalytic supports in heterogeneous photocatalysis [14]. Thus, nearly 82–99.5 % dye degradation under visible radiation using copper oxide nanoparticles supported onto nanozeolites (nSOD, nANA, nX, NaX) are reported in the literature [15–18].

At the same time, growing concern about environmental pollution is driving the search for innovative and sustainable solutions, with the development of green metal nanoparticles (MNPs) for application in environmental remediation, offering effective and more environmentally friendly methods for wastewater treatment. Green MNPs are materials with dimensions between 1 and 100 nm with specific properties [19], such as greater surface area and porosity, and high reactivity. They are prepared by green synthesis using biomolecules from plant extracts (e.g. *Camellia sinensis* extract), which act as reducing and stabilizing agents, transforming metal ions into nanoparticles in a simple, economical way, and with a lower environmental impact [20]. Thus, this approach aligns with the principles of green chemistry, seeking to minimize waste generation and the use of hazardous substances. Among the main applications of NMPs is environmental remediation, where these nanomaterials have been used in wastewater treatment through heterogeneous photocatalysis under visible radiation to catalyze degradation reactions of complex organic pollutants, such as dyes [21,22].

Despite the demonstrated photocatalytic efficiency of heterogeneous supported nanocatalysts for synthetic dye degradation (characterized by high degradation rates, catalyst stability, and selectivity) few studies have explored the application of this process at pilot-plant or industrial scale [23]. Furthermore, beyond photocatalytic efficiency, other important parameters such as energy consumption, cost-effectiveness, catalyst reusability, environmental impact, and operational feasibility should be considered to deepen the understanding of wastewater treatment performance. Thus, some studies emphasize eco-friendly synthesis methods and process optimization to enhance the treatment of complex industrial wastewater, highlighting advantages of green nanocatalysts regarding sustainability and adaptability to real effluents [24]. Conversely, the advances in heterogeneous nanocatalysts for photocatalytic degradation of food dyes are deeply highlighted in the literature reviews about catalysis [25], discussing catalyst performance, reaction mechanisms, and challenges related to scale-up.

Thus, to address this research gap, comprehensive studies encompassing batch-scale energy consumption, economic analysis, and scale-up feasibility are essential to verify the practical applicability of different nanocatalysts in wastewater treatment at industrial levels.

Economic analysis techniques such as Net Present Value (NPV), Internal Rate of Return (IRR), Return on Investment (ROI), and Discounted Payback Period (DPP) are essential for assessing the financial feasibility of projects [26]. NPV calculates the difference between future cash flows discounted to present value and the initial investment, with a positive result indicating project viability [27]. IRR represents the discount rate that makes the NPV equal to zero, meaning the higher it is relative to the minimum acceptable rate of return, the more attractive the project [28]. ROI measures investment profitability, calculated as the ratio between net profit and investment cost, making it useful for comparing different opportunities [29]. Discounted Payback, on the other hand, indicates the time required to recover the initial investment while considering the value of money, making it more accurate than simple payback [30]. To apply these techniques, it is essential to have information such as the initial investment, estimated future cash flows, discount rate (or cost of capital), and analysis period. These tools support decision-making by comparing projects, quantifying risks, and optimizing resource allocation [31].

Allied with this approach, computational tools (e.g., Exploratory Data Analysis – EDA) have proved to be helpful in getting information about the process and to correlate the variables of the wastewater treatment to optimize pollutant removal (%R) [32,33]. Thereafter, EDA is suitable for addressing the main variables affecting the process and identify patterns within data [34]. In this sense, EDA reduces costs and time associated with further experimental procedures in optimization processes [35].

In this view, the present work aims to evaluate an economic analysis of the synthesis of a green nanocatalyst (copper oxide nanoparticles supported onto sodalite nanozeolite, nSOD@CuO-NPs) and the Exploratory Data Analysis (EDA) analysis of experimental data to explore key factors that affect/optimize the binary dye mixture degradation under visible radiation.

2. Materials and methods

2.1. Nanocatalyst synthesis

The heterogeneous nanocatalyst (a nanocomposite) consisted of copper oxide nanoparticles (CuO-NPs) as the reinforcement and the sodalite nanozeolite (nSOD) as the matrix, published in previous work [36]. The nSOD was obtained by hydrothermal synthesis using solid (agro)industrial residues as raw materials, while CuO-NPs were prepared by green synthesis using green tea (*Camellia sinensis*) as a reducing agent. The nSOD@CuO-NPs were then synthesized by the impregnation method, with 3 % wt. of CuO-NPs incorporated into the nSOD. Detailed information about the development of the supported nanocatalyst is available in a study published by the research group [36].

2.2. Characterization techniques

To evaluate the crystalline phases, X-ray diffraction (XRD) was performed using a Bruker diffractometer (model D2 Advance) with a copper tube ($\lambda_{Cu\text{-}\alpha}$ = 0.15418 nm). Attenuated Total Reflectance-Fourier Transform Infrared (ATR-FTIR) was applied to identify functional groups using an IRPrestige-21 spectrophotometer (Shimadzu, Japan), with a resolution of 4 cm^{-1} in the range of 450 to 4000 cm^{-1}. The morphological characteristics and elemental composition were analyzed using Field Emission Gun Scanning Electron Microscopy (FEG-SEM) in a TESCAN MIRA3 Scanning Electron Microscope with OXFORD Xplore EDS Detector operating at an acceleration voltage of 15 kV with a working distance of 25 mm. For N_2 porosimetry, the equipment (Gemini VII 2375 Surface Area Analyzer Micrometrics) was used (P P_0^{-1} = 0.0–1.0) and the textural properties (S_{BET}, D_p an V_p) were evaluated by the Brunauer-Emmett-Teller (BET) and Barret-Joyner-Halenda (BJH) methods. Diffuse Reflectance Spectroscopy (DRS) analysis was carried out in a JASCOV-670 spectrometer (λ = 200–800 nm). The zero charge point (pH_{ZCP}) was evaluated by 11-point assays, using NaOH (0.1 mol L^{-1}, ACS reagent, ≥97.0 %, pellets, Sigma-Aldrich®) and HCl (0.1 mol L^{-1}, ACS reagent, 37 %) for pH adjustments. Malvern-Zetasizer® (model nano ZS, ZEN3600 -United Kingdom) was used to determinate the surface charge by zeta potential (ZP). Detailed information on characterization techniques is available in a study published by the research group [36].

2.3. Photocatalytic assay

The heterogeneous photocatalysis was carried out under visible radiation using a mixture of CV and MB dyes at two total concentrations: 70 mg L^{-1} and 135 mg L^{-1}. These concentrations were selected based on reported values from real textile wastewater samples found in the literature. Thus, to prepare the CV:MB dye mixtures, equal masses (1:1 w w^{-1}) of each dye were used (3.5 mg for the 70 mg L^{-1} solution and 6.75

mg for the 135 mg L^{-1} solution), each dissolved separately in beakers containing 50 mL of distilled water. The two solutions were then combined to yield a total volume of 100 mL of dye mixture. Due to the different molecular weights of the dyes ($M_W = 407.9797$ g mol^{-1} for CV and $M_W = 319.85$ g mol^{-1} for MB), the molar fractions of the mixture were calculated as 44 % CV and 56 % MB.

The solution pH (4–10) and nanocatalyst concentration ([nSOD@-CuO-NPs] = 0.5–1.5 g L^{-1}) range were selected based on an optimization study published by the research group [36].

The photodegradation reactions was performed in a slurry reactor under visible irradiation (Empalux® Bulb LED Lamp, 50 W Halogen Equivalent with 600 W m^{-2} as the maximum radiations and wavelength ranging from 275 to 950 nm) in two steps; (a) in dark condition: adsorption of dyes molecules onto the catalytic surface without irradiation (~60 min), and (b) photocatalytic degradation of the dyes: under visible radiation and a distance of about 20 cm from the LED lamp and sample, aliquots (~3 mL) were collected at time 0, 15, 30, 45, 60, 75, 90, 105, 120, 150, 180, 210 and 240 min, centrifuged (4500 rpm for 15 min), and diluted in distilled water (1:15 v v^{-1}) for absorbance reading in the spectrophotometer UV–Vis (Shimadzu) at $\lambda = 590$ nm (CV) and $\lambda = 663$ nm (MB). The dye removal (%R) was evaluated according to Eq. (1).

$$\%R = \left(\frac{A_0 - A_t}{A_0}\right) \times 100 \quad (1)$$

where: A_0 is the initial absorbance ($t = 0$) and A_t is the absorbance at time t.

The apparent rate constant of the pseudo-first-order reaction (k) was evaluated by linear regression of the Langmuir-Hinshelwood (L-H) model according to Eq. (2) [37,38].

$$\ln\left(\frac{C_{i0}}{C_i}\right) = k^{*}t \quad (2)$$

where: C_{i0} is the initial dye concentration (mg L^{-1}); C_i is the dye concentration at time t (mg L^{-1}), k is the apparent rate of the pseudo-first-order reaction (min^{-1}); and t is the reaction time (min).

The curve fitting of data to the L-H model was determined by the determination coefficient (R^2) as the objective function, and the Root Mean Squared Error (RMSE) as the loss function, according to Eqs. (3)–(4) [39].

$$R^2 = 1 - \frac{\sum_{i=1}^{N}\left(y_{i,exp} - y_{i,pred}\right)^2}{\sum_{i=1}^{N}\left(y_{i,exp} - \widehat{y}_{i,pred}\right)^2} \quad (3)$$

$$RMSE = \sqrt{\frac{\sum_{i=1}^{N}\left(y_{i,exp} - \widehat{y}_{i,pred}\right)^2}{N}} \quad (4)$$

where: $y_{i,exp}$ is the observed values (experimental data) for the i^{th} observation; $y_{i,pred}$ is the predicted data associated with the response ($\ln(C_{i0}\,C_i^{-1})$); $\widehat{y}_{i,pred}$ is the predicted value for the i^{th} observation and N is the number of observations.

Table 1 shows the dataset used to implement Exploratory Data Analysis (EDA), which is a crucial step prior to the scale-up process.

According to Table 1, the nanocomposite were used to evaluate photocatalytic activity and the effect of the reactor volume on CV:MB dye degradation. Moreover, high concentration values for CV:MB dye mixture were selected considering the characteristics of real textile wastewater systems [40].

2.4. Exploratory data analysis

To identify optimized conditions and estimate the cost associated with the heterogeneous photocatalysis, an Exploratory Data Analysis (EDA) was carried out in Python 3.4.11 using NumPy, Pandas, Matplotlib/Seaborn, and SciPy libraries. The data obtained from the photocatalytic assay (Table 1) were used as the dataset. It is worth pointing out that each of the 12 runs reported in Table 1 is subdivided into approximately 12 points ranging from 0 to 240 min, measured at three wavelengths ($\lambda = 590$, 630, and 663 nm), resulting in 36 data lines per run. Consequently, for the 12 runs, the dataset was organized into a spreadsheet comprising approximately 400 rows and 15 columns, which is available on GitHub (https://github.com/LeandroOviedo/Machine-and-Deep-Learning, file Volume_and_cost_analsysis-WWT.xlxs). Thus, the variables dye concentration ([CV:MB]), pH, reaction time (t_{rxn}), nanocatalyst concentration ([nSOD@CuO-NPs]), reactor volume ($V_{reactor}$) and were selected for investigation. These variables were further correlated with dye removal (%R) in the wastewater treatment at laboratory scale.

Table 1
Dataset used in heterogeneous photocatalysis under visible radiation.

Experiment	Reactor volume (mL)	pH	[Nanocatalyst] (g L^{-1})	[CV:MB] (mg L^{-1})
1	100	8	0.5	70
2	100	8	0.8	70
3	100	4	1.0	70
4	100	8	1.5	70
5	100	10	1.5	70
6	100	4	0.8	135
7	100	7	0.8	135
8	100	10	1.5	135
9	250	10	1.5	70
10	500	10	1.5	70
11	1000	10	1.5	70
12	1000	8	1.5	135

Additionally, total costs (CT) involved in bench scale (operational, raw material and nanocatalyst production costs, COP, CRM and CNP) were the variables. The EDA were carried out using data visualization, normality test, and correlation analysis of the data. In this sense, valuable insights can be obtained for scaling up the heterogeneous photocatalysis from laboratory to industrial scale, in which 10, 20, and 30 m^3 of dye-contaminated wastewater can be treated.

2.5. Economical analysis and scale-up

2.5.1. Acquisition cost evaluation

Aiming to apply the heterogeneous photocatalysis process on an industrial scale, the investment cost of the necessary raw materials for scale-up was estimated using the Lang factor method, according to Eq. (5) [41]. This equation is useful for estimating the investment cost for a chemical plant.

$$C_{TM} = F_{Lang}\sum_{i=1}^{n} C_{p,i} \quad (5)$$

where: C_{TM} is the total cost required to establish the plant (US$); $C_{p,i}$ is the acquisition cost of the main pieces of equipment (US$); n is the total number of individual units and F_{Lang} is the Lang factor (3.63 for fluid and solids processing).

Eq. (5) utilizes Lang factors as a multiplying variable. However, this method is not sensitive to changes in process configuration. It is common to estimate the cost (in dollars) based on a specific capacity variable (e.g., reactor volume). Thus, the economic analysis was performed considering the amount of nSOD@CuO-NPs required to treat 10, 20, and 30 m^3 of dye-contaminated wastewater. Moreover, Fig. S1 shows a complete flowchart of the proposed process of nanocatalyst synthesis and tertiary treatment by heterogeneous photocatalyst at pilot-plant/industrial scale. Information on all costs involved in implementing the wastewater treatment plant is in the supplementary information.

2.5.2. Production cost evaluation

Production cost evaluation (C_P) involves fixed investment costs (C_{FI}), labor costs (C_L), utility costs (C_{UT}), wastewater treatment costs (C_{WT}), and raw material costs (C_{RM}). Thus, detailed information on these costs is provided in Table S1.

The values set for each parameter were selected within the range of typical values reported/expected in the literature. Moreover, the DC, FC and GC can be summed up and expressed as seen in Eqs. (6)–(8):

$$DC = C_{RM} + C_{UT} + C_{WT} + 1.31{*}C_L + 0.17{*}C_{FI} + 0.03{*}C_P \quad (6)$$

$$FC = 0.155{*}C_{TM} + 0.702{*}C_L \quad (7)$$

$$GE = 0.1755{*}C_L + 0.0075{*}C_{FI} + 0.13{*}C_P \quad (8)$$

Thereafter, the total production cost (C_{TP}) can be expressed as Eq. (9):

$$C_{TP} = DC + FC + GE \quad (9)$$

Combining Eqs. (7) and (8) and substituting them in Eq. (9):

$$C_{TP} = C_{RM} + C_{UT} + C_{WT} + 2.1875{*}C_L + 0.3325{*}C_{FI} + 0.16{*}C_P \quad (10)$$

where: C_{TP} is the total production cost; C_{RM} corresponds to the raw material costs; C_{UT} represents the utility cost; C_{WT} is the waste treatment costs; C_L is the labor costs; C_{FI} is the fixed investment cost and $C_P$is the production cost evaluation.

Eq. (10) informs the total cost of investment (C_{TP}) to synthesize the nSOD@CuO-NPs nanocatalyst for use in a heterogeneous photocatalysis system at pilot-plant/industrial scale for organic pollutants degradation under visible radiation.

2.5.3. Cash flow analysis

Net present value (NPV), internal rate of return (IRR) and Discounted Payback Period (DPP) were used as cash flow analysis methods. NPV (Eq. (11)) measures the present value of future cash flows discounted at a minimum attractive rate, indicating whether a project generates value, whereas the IRR (Eq. (12)) represents the rate of return on investment and is useful for comparing different projects. The DPP (Eqs. (13) and (14)) measures the time required to recover the initial investment using discounted cash flows, accounting for the time value of money. In contrast to the traditional Payback, it reflects the true financial risk and profitability of an investment [42]. However, the D_P was used in this work and considers the time value of money, correcting the limitation of traditional payback. Additionally, the cost-benefit (C/B), described by Eq. (15), is calculated to verify how much money will be returned for each invested dollar in a project [43]. Table 2 shows all the information about each cash flow analysis method.

The economic analysis was performed considering three production scenarios (15, 30, and 45 kg day^{-1}), with SiO_2 being purchased from China. The analysis estimated the cost of equipment, production cost, and gross profit, and calculated the cash flow from these values. The option for purchasing SiO_2 was due to the low yield in silica extraction from rice husks using chemical and thermal treatments (ca. 20 %) [44].

An important consideration in the cost estimation for obtaining Al_2O_3 from alum sludge was that only the pretreatment processes, specifically drying and calcination, were included. The untreated alum sludge was provided free of charge through local partnerships, so the estimated cost reflects solely the processing required to convert the residual sludge into a usable Al_2O_3 source.

The economic analysis was expressed in US$ dollars as the monetary unit, dedicated to the cost correlations available in the literature [45]. Thus, considering only the investment cost, the four scenarios were structured as follows:

- Production of 15 kg day^{-1} of nanocatalyst: capacity to treat 10 m^3 of wastewater;
- Production of 30 kg day^{-1} of nanocatalyst: capacity to treat 20 m^3 of wastewater;
- Production of 45 kg day^{-1} of nanocatalyst: capacity to treat 30 m^3 of wastewater.

Table 2
Detailed information about the cash flow methods used in this work.

Cash flow method	Equation	Meaning
NPV	$NPV = \sum_{t=0}^{n} \frac{FC_t}{(1+r)^t} - I_0$ (11) where: FC_t = cash flow at time t r = discount rate (cost of capital or required return) t = period (years, months, etc.) n = total number of periods I_0 = initial investment	calculates the present value of future cash flows, discounted at a required rate of return (r) If NPV > 0, the project is profitable If NPV < 0, the project is not financially viable If NPV = 0, the project breaks even
IRR	$0 = \sum_{t=0}^{n} \frac{FC_t}{(1+IRR)^t} - I_0$ (12) where: FC_t = cash flow at time t IRR = internal rate of return t = period (years, months, etc.) n = total number of periods I_0 = initial investment	IRR is the discount rate that makes the NPV equal to zero If IRR > r, the project is financially viable If IRR < r, the project should be rejected Where r is the required return
DPP	$FC_{discounted} = \sum_{t=0}^{n} \frac{FC_t}{(1+r)^t}$ (13) Then, sum the discounted cash flows until the initial investment is fully recovered: $FC_{discounted} \geq I_0$ (14)	Unlike the simple Payback Period, this method considers the time value of money. It determines how long it takes to recover the initial investment using discounted cash flows and provides a more accurate risk assessment than the traditional payback method Steps of DPP: a) Discount each cash flow using the required rate of return; b) Cumulatively sum the discounted cash flows; c) Identify the year when the investment is fully recovered.
C/B	$C/B = \frac{VPL}{\text{Investment cost}}$ (15)	C/B > 1 (Benefits exceed costs): Reliable project C/B < 1 (Costs are higher than benefits): Reliable project

Table S2 presents some parameters considered in the economic analysis calculation. According to Table S2, the total cost of investing in the chemical plant and expenses over the year was dependent on the number of operators, supervisors, and working capital, with the profit considering an interest rate (12 % in this study). It should be noted that the cost calculation did not consider operational risks or fluctuations in raw material prices.

3. Results and discussion

3.1. Characterization of the nSOD@CuO-NPs

nSOD@CuO-NPs showed a mesoporous structure with analcime, sodalite, cuprite, and tenorite crystalline phases identified by X-ray Diffraction (XRD), stability in aqueous solution by zeta potential (ZP = −18.5 ± 1.0 mV), and optical activity by Diffuse Reflectance Spectroscopy (DRS) (E_g = 1.38 eV). Additionally, the nanocatalyst showed textural properties ($S_{BET} = 14.8 \pm 0.73$ m^2 g^{-1}, $V_p = 0.037 \pm 0.001$ cm^3 g^{-1}, $D_p = 16.6 \pm 0.71$ nm), zero charge point (pH_{ZCP}) at pH 7.65, and the chemical composition: C (23.7 %), O (41.1 %), Si (10.6 %), Na (8.8

%), Al (8.4 %), Fe (4.0 %), Cu (2.1 %), respectively. Furthermore, these properties are interesting and attractive in the field of heterogeneous photocatalysis, focused on the photocatalytic degradation of recalcitrant organic pollutants (synthetic dyes, pesticides, herbicides, drugs and microplastics). Moreover, the nSOD@CuO-NPs is a green nanocatalyst that can be successfully obtained from plant extract and solid (agro) industrial waste. Detailed information on the characterization results and discussion of the supported nanocatalyst are available in a study published by the research group [36].

3.2. Exploratory data analysis (EDA)

3.2.1. Effect of the dye concentration on the absorbance readings

To explore the effect of dye concentration (mono and bicomponent system) on the absorbance readings, the dyes were analyzed using a UV–Vis spectrophotometer. The results are present in Fig. 1.

According to Fig. 1, in monocomponent systems, the organic dyes show maximum light absorption at $\lambda = 590$ nm and 664 nm, respectively. However, in a bicomponent system (CV:MB dye mixture), a slight shift in the characteristic wavelength of MB dye was observed (from 664 to 663 nm), followed by an increase in absorption intensity. Additionally, a new characteristic wavelength is noticeable, probably due to the high concentration of the organic dyes, which can result in either dye molecule aggregation (e.g., interaction of CV and MB dye by π-π stacking or electrostatic forces) or dimerization of the MB dye molecule [46]. In this work, three wavelengths ($\lambda = 590$, 630, and 663 nm) and high concentrations (70 and 135 mg L^{-1}) were used for absorbance readings and photocatalytic degradation.

Thus, the scanning present in Fig. 1 proved the coherence of the methodology used in this work with the experimental observations found in the literature. Thereafter, this analysis confirmed the use of the proposed methodology for further studies dealing with crystal violet and methylene blue dyes in bicomponent systems.

3.2.2. Heterogeneous photocatalysis: exploratory data analysis

Initially, normality tests and correlation analysis of photocatalytic parameters and experimental observations were carried out. Since the sample size ($N = 400$) was greater than 30, the Kolmogorov-Smirnov test was employed to verify the normal distribution of the data [47,48]. The normality test indicated that all variables showed a non-normal distribution, evidenced by p-values ($p < 0.001$). Therefore, a non-parametric method for correlation analysis was recommended. Hence, the Spearman method was employed. Fig. 2 shows the results of the Spearman correlation, while Table S3 reports the results of the normality test.

According to Fig. 2, the Spearman correlation analysis revealed that the dye removal (%R) exhibited moderate and positive correlations with several variables. Specifically, dye removal (%R) shows a correlation coefficient of $\rho = 0.45$ with [nSOD@CuO-NPs], indicating a notable relationship between the dye removal (%R) and the concentration of nanoparticles. Thus, an increase in the nanocatalyst concentration ([nSOD@CuO-NPs]) should increase the dye removal (%R). This observation is consistent with previous studies reporting that higher catalyst loadings enhance the availability of active sites, promoting more efficient reactive species generation and subsequently improving dye degradation rates [49]. For instance, increasing CuO-NPs concentrations have been shown to accelerate the photodegradation kinetics of organic dyes by facilitating greater adsorption and surface redox reactions.

Similarly, dye removal (%R) correlates positively (a moderate correlation) with pH ($\rho = 0.43$) and $V_{reactor}$ ($\rho = 0.40$), suggesting that both the reactor volume and pH influence the removal efficiency. Moreover, it was observed in the experimental runs that an increase in $V_{reactor}$ resulted in higher dye removal (%R) values. This trend is observed in an experimental study of ozonation, where the reactor volume was crucial to the performance of the AOP process for the degradation of insecticides. Thus, the study revealed that higher reactor volumes achieved nearly 90 % degradation using a smaller amount of nanocatalyst and a lower radiation dose compared to smaller reactor volumes [50].

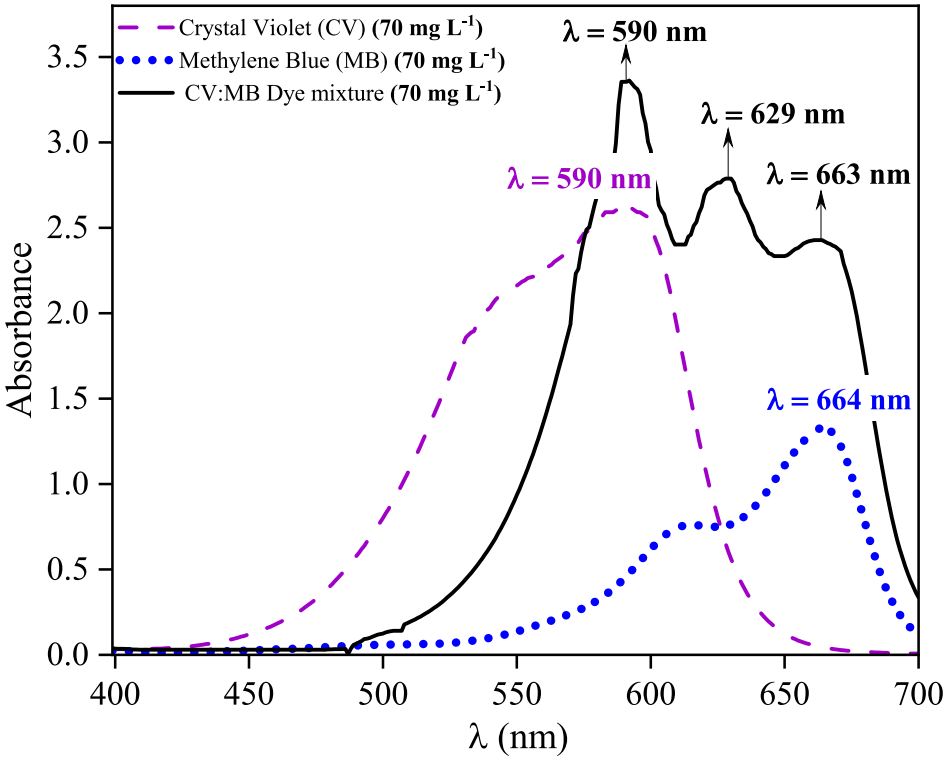

Fig. 1. UV–Vis spectra for CV and MB dyes in mono and bicomponent systems.

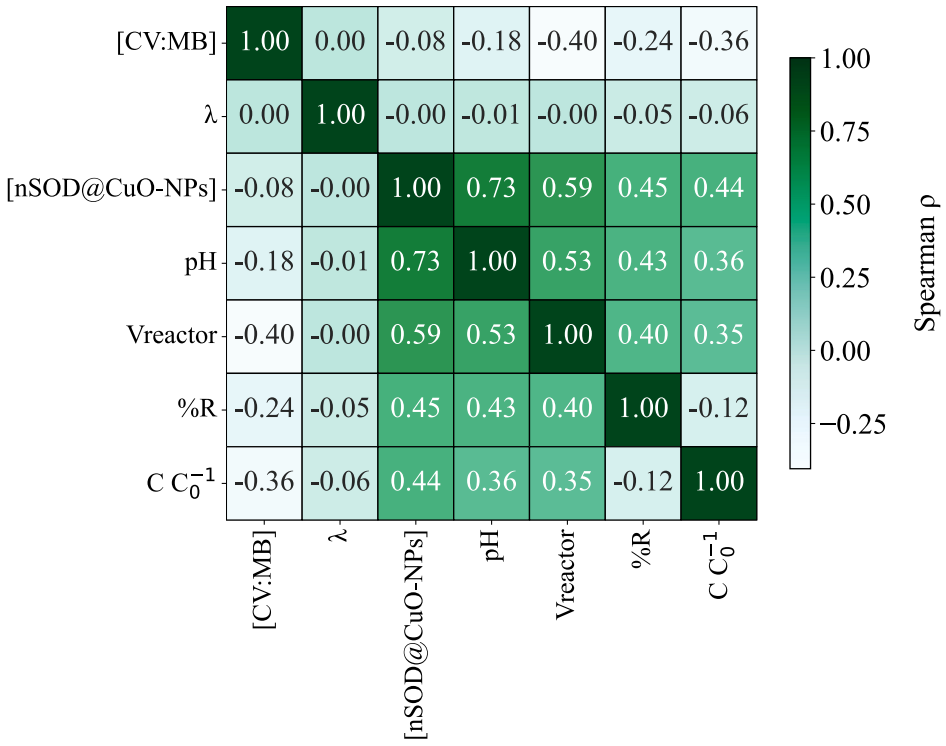

Fig. 2. Spearman correlation for experimental data.

The findings suggest a positive relationship between the increased effective reactor volume and the enhanced degradation efficiency.

Regarding the pH, several recent studies have demonstrated that an increase in pH generally enhances the photocatalytic degradation efficiency of organic pollutants, particularly dyes, due to favorable changes in surface charge, pollutant ionization state, and reactive species generation. For instance, a recent report revealed that alkaline conditions improved the degradation rate of MB by increasing the availability of hydroxyl radicals, which are key reactive species in photodegradation mechanisms [51]. Thus, increasing the pH favors the photocatalytic degradation of methylene blue dye, showing better adsorption and enhanced degradation under alkaline or optimized pH conditions.

Therefore, it is expected that higher volumes and pH (from neutral to alkaline) will result in higher degradation percentage of CV and MB dyes. In contrast, weaker correlations are observed between λ ($\rho = 0.24$) and dye removal (%R), indicating that dye molecules (identified by characteristic wavelength) show a lower effect on dye removal (%R) under the conditions studied. It was due to the CV and MB showing some similarities, such as structure and electrical nature (cationic dyes) [52].

Fig. 3 explores the effect of nanocatalyst concentration and reaction time on the dye removal (%R), whereas Fig. 5 depicts the effect of solution pH and wavelength on dye removal (%R).

According to Fig. 3, the EDA revealed that the dye removal increases with the increase of the nanocatalyst concentration (in all wavelengths), probably due to higher availability of active sites for the degradation reaction. Thus, nSOD@CuO-NPs adsorbs CV and MB dye molecules and mineralizes them to CO_2 and H_2O by $^{\bullet}OH$ and $^{\bullet}O_2^-$ generation [53]. However, some threshold value for nanocatalyst concentration to achieve significant degradation is reported in the literature (ca. 0.5–2.0 g L^{-1}) [54]. Despite the high nanocatalyst concentration used at optimal

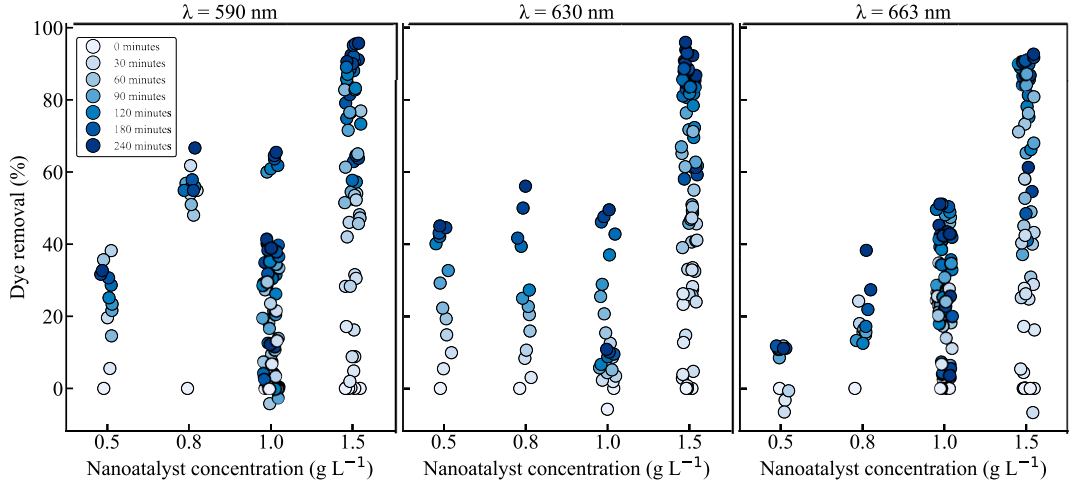

Fig. 3. Effect of the nanocatalyst concentration and reaction time on dye removal (sample size (N) for nanocatalyst concentration: 0.5 g L^{-1} ($N = 51$), 0.8 g L^{-1} (N = 51), 1.0 g L^{-1} ($N = 122$), 1.5 g L^{-1} ($N = 176$)/$V_{reactor}$ = 100 mL | $T = 25 \pm 2$ °C | $y_{CV} = 0.44$ and $_{yMB} = 0.56$ | under visible radiation with 600 W m^{-2}).

conditions ([nSOD@CuO-NPs] = 1.5 g L^{-1}), %R > 80 are reported by experimental data, probably attributed to the high dye mixture concentration, which is expressively high ([CV:MB] = 70 mg L^{-1}).

Furthermore, there was a noticeable increasing trend in %R as time elapsed. Specifically, as the reaction time increases, the %R tends to increase, suggesting that longer reaction times promote more effective dye removal. This trend is most apparent at the highest nanocatalyst concentration (1.5 g L^{-1}), where the shift from lighter to darker shades of blue indicates a progressive increase in %R with time.

In parallel, according to Fig. 4, higher pH values generally result in a greater percentage of dye removal. It can be attributed to higher reactive oxygen species (e.g., •OH, $•O_2^-$) generation and to the surface charge of nSOD@CuO-NPs at alkaline pH (pH > pH_{ZCP}) [55]. In the latter case, the nanocatalyst surface is deprotonated, resulting in higher attractive electrostatic forces between nSOD@CuO-NPs and CV/MB molecules, which are cationic dyes [56].

In addition, it is worth pointing out that in all cases, the systems consist of a binary dye mixture. Thus, at λ = 590 nm, CV is treated as the target pollutant, whereas MB is treated as an interferent. On the contrary, at λ = 663 nm, MB is the target pollutant and CV is treated as an interferent. Finally, at λ = 630 nm, both CV and MB are considered the target pollutants, with no interferents. In this sense, the focus relies on both dyes interchangeably. Based on Fig. 3, lower removal was reported for CV and MB at pH 4 since they are protonated at acidic pH, resulting in higher electrostatic repulsion forces between them and the nanocatalyst surface (pH_{ZCP} 7.65) [57,58]. In addition, as pH increased from 7.0 to 8.3, higher %R is reported for both dyes, with nSOD@CuO-NPs showing higher selectivity for CV dye.

At pH 10, nSOD@CuO-NPs showed high %R (80–95 %) for CV and MB dyes, interchangeably. Thus, it was noticeable that dye removal is more favorable at pH 10 for all wavelengths. According to these findings, [nSOD@CuO-NPs] = 1.5 g L^{-1} and pH 10 can be selected as the optimal conditions for the CV:MB photocatalytic degradation after 240 min under visible radiation and concentrated binary systems, such as [CV:MB] = 70 mg L^{-1}. Therefore, these conditions were further considered in the economic analysis presented in Section 2.3. For a comprehensive overview of the experimental results, detailed numerical data for all conditions tested are presented in Table 3.

According to Table 3, lower concentrations (70 mg L^{-1}) favored wastewater treatment, yielding higher removal percentages (%R). This outcome can be attributed to the reduced competition for active sites on the photocatalyst at lower dye concentrations, allowing more efficient interaction between the dye molecules and the catalyst [59]. Additionally, the photocatalytic activity of nSOD@CuO-NPs exhibited an increasing trend in %R as the nanocatalyst concentration increased from 0.5 to 1.5 g L^{-1}, with a strong dependency on the solution pH. Notably, as discussed earlier, the optimal conditions for CV:MB photodegradation were identified as an alkaline medium (pH 10), a nanocatalyst concentration of 1.5 g L^{-1}, and a dye concentration of 70 mg L^{-1}. Thereafter, Fig. 5 shows the degradation curve for CV:MB degradation at λ = 590, 630, and 663 nm and optimized conditions.

The results in Fig. 5 indicate that the degradation of CV and MB dyes follows pseudo-first-order kinetics, as described by the Langmuir-Hinshelwood model. Moreover, CV dye showed a faster degradation (k = 0.0144 min^{-1} at λ = 590 nm) than MB dye (k = 0.0131 min^{-1} at λ = 663 nm), probably due to differences in molecular structure and interaction with the nanocatalyst [60]. The mixture mole fractions (y_{CV} = 0.44, y_{MB} = 0.56) further highlight the competitive adsorption and degradation dynamics between CV and MB, which is consistent with literature reports on photocatalytic degradation of CV and MB dyes in bicomponent systems under visible light radiation [61]. In addition, an intermediate value of k was reported for CV:MB at λ = 630 nm. To

Table 3
Dataset used in heterogeneous photocatalysis under visible radiation.

Reactor volume (mL)	pH	[Nanocatalyst] (g L^{-1})	[CV:MB] (mg L^{-1})	%R (λ = 590 nm)	%R (λ = 630 nm)	%R (λ = 663 nm)
100	8.30	0.5	70	32.66	20.59	11.11
100	8.31	0.8	70	12.27	19.94	25.52
100	3.96	1.0	70	38.73	49.52	42.79
100	8.26	1.0	70	66.67	63.36	38.28
100	8.29	1.5	70	82.33	80.69	83.37
100	10.21	1.5	70	84.53	88.01	86.75
100	3.96	0.8	135	34.97	39.01	43.42
100	7.10	0.8	135	41.42	10.84	3.59
100	10.21	1.5	135	64.60	61.17	61.28
250	10.08	1.5	70	92.43	93.86	86.82
500	10.14	1.5	70	90.60	92.29	91.05
1000	10.11	1.5	70	95.70	95.94	92.89
1000	10.22	1.5	135	83.40	81.34	80.27

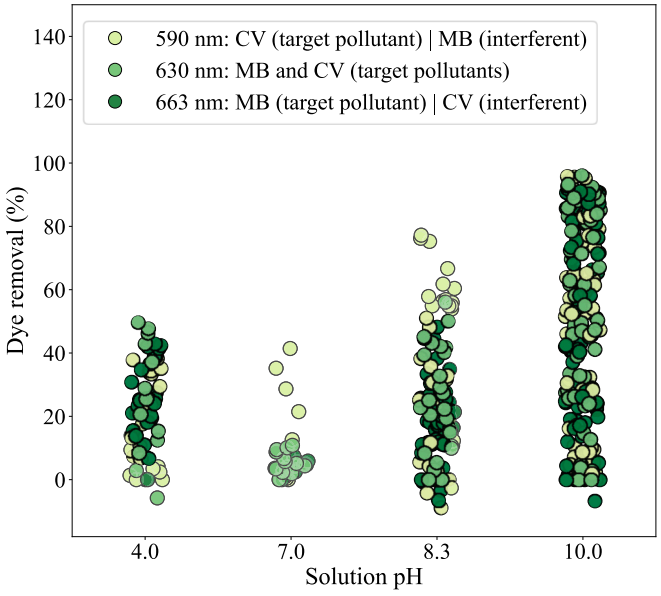

Fig. 4. Effect of the pH and wavelength on dye removal. (Sample size (N): pH 4 (N = 35), pH 7 (N = 53), pH 8.3 (N = 136), pH 10 (N = 176)/$V_{reactor}$ = 100 mL | T = 25 ± 2 °C | y_{CV} = 0.44 and $_{yMB}$ = 0.56 | under visible radiation with 600 W m^{-2}).

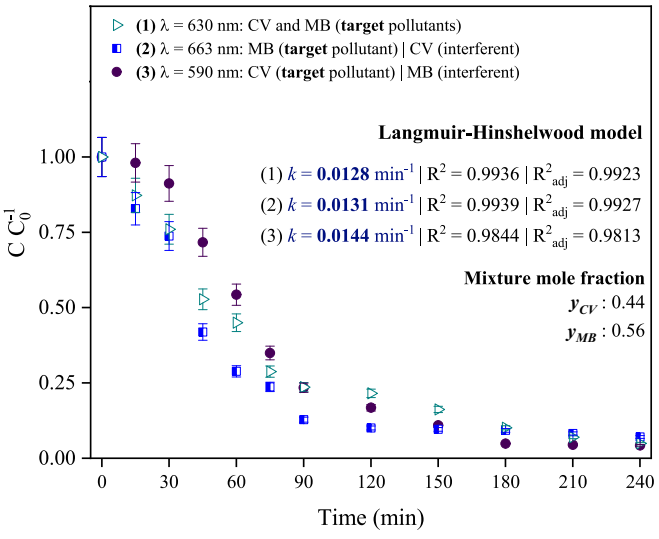

Fig. 5. Degradation curve and Langmuir-Hinshelwood regression parameters. ([nSOD@CuO-NPs] = 1.5 g L^{-1} | [CV:MB] = 70 mg L^{-1} | pH 10 | Vreactor = 1.0 L | under visible radiation with 600 W m^{-2}).

investigate the effect of the reactor volume on the dye removal (%R) by heterogeneous photocatalysis (Fig. 6), EDA was applied to experimental data regarding different reactor volumes.

According to Fig. 6, there was an increase in dye removal (%R) with the variation of the reactor from 100 to 1000 mL. It was probably due to the increase in residence time and better distribution of the dye molecules and nanocatalyst inside the reactor [62]. Moreover, higher degradation for CV than MB was reported, which can be attributed to the differences in molecular structure, charge, and optical properties between CV and MB dyes. Crystal violet (CV) has a higher molecular weight and more complex aromatic structure, which enhances its interaction with the nanocatalyst surface through π-π stacking and electrostatic forces [63]. Additionally, CV exhibits stronger absorption in the visible spectrum, facilitating greater photocatalytic activation under visible radiation [64,65]. In contrast, methylene blue (MB) has a simpler structure and lower affinity for the nanocatalyst surface, resulting in comparatively reduced degradation efficiency [66]. Furthermore, from 100 to 1000 mL, the increase in dye removal (%R) were around 8.9 %, 20.3 %, and 21.8 % for λ = 630, 663, and 590 nm were, respectively.

The observed increase in dye degradation percentage with increasing solution volume from 100 to 1000 mL can be attributed to several factors. A larger volume provides an extended residence time, allowing the dye molecules more opportunity to interact with the photocatalyst and undergo degradation. Additionally, increased volume promotes better spatial distribution of both the dye molecules and the photocatalyst particles, enhancing contact efficiency. This can reduce local saturation effects on the catalyst surface, improving overall photocatalytic activity. Moreover, the larger medium may facilitate more uniform light penetration and absorption, boosting the generation of reactive oxidative species responsible for dye breakdown. Together, these factors contribute to the enhanced removal efficiency observed at higher volumes.

Based on these findings, an economic analysis for a laboratory-scale heterogeneous photocatalysis system was evaluated. For this, the treatment of 1.0 L of an aqueous solution contained the CV:MB dye mixture operating in batch mode under 25 ± 2 °C at the optimal condition (pH 10, [CV:MB] = 70 mg L^{-1}, [nSOD@CuO-NPs] = 1.5 g L^{-1}). Additionally, for this analysis, it was considered that the availability of the main pieces of equipment required to perform the wastewater treatment (e.g., small-scale furnace with T_{max} = 1000 °C and P = 4 kW; oven with air circulation – 600 L; Small-scale ball mill, photocatalytic reactor – 1.0 L, centrifuge, UV–Vis spectrophotometer). In addition, the cost of the nanocatalyst characterization and maintenance of the reactor was included. In total, the investment cost considered here varies from US$ 33,043.64 to US$ 35,043.64. Moreover, Fig. S2 informs the cost estimation of the wastewater treatment for the binary system investigated in this work, excluding the investment cost associated with the laboratory equipment. The energetic cost (variable cost) at laboratory scale ($V_{reactor}$ = 1.0 L) was calculated combining the power of the magnetic stirrer and the lamp used for the photodegradation, according to Eq. (16).

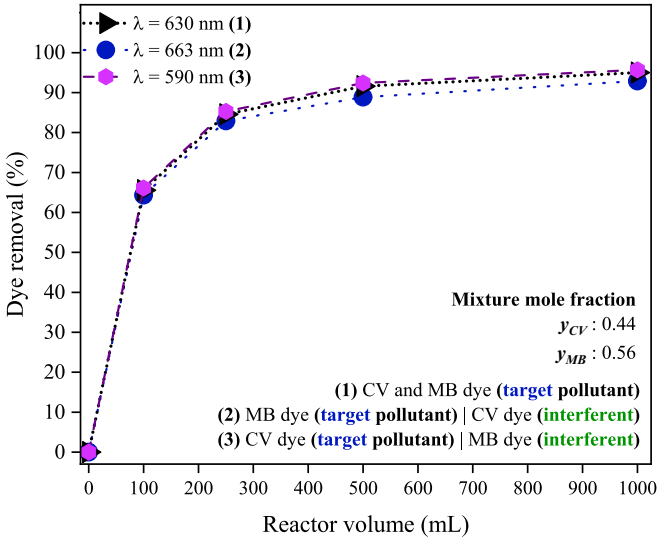

Fig. 6. Effect of the reactor volume on dye removal. ([nSOD@CuO-NPs] = 1.5 g L^{-1} | [CV:MB] = 70 mg L^{-1} | pH 10 | $V_{reactor}$ = 1.0 L | under visible radiation with 600 W m^{-2}).

$$EC = 1.10^{*}t_{op} + 0.5^{*}t_{op} \quad (16)$$

where: t_{op} is the operation time of the heterogeneous photocatalysis (hours), which varied from 0 to 4 h; the values 1.10 and 0.5 correspond to the energy consumption (in kWh) of the magnetic stirrer and lamp, respectively.

According to Fig. S2, the energetic cost required to treat 1.0 L of wastewater containing CV:MB dye mixture varied from US$ 0.00 (at 0 min) to US$ 6.40 (after 240 min of heterogeneous photocatalysis under visible radiation). However, to estimate the total cost used to treat wastewater, the energetic cost should be added to the costs associated with raw materials acquisition and nanocatalyst production and the reuse capacity of the nanocatalyst provided, which yields to higher values. Thereafter, to explore the viability of the implementation of this wastewater treatment, the economic analysis was extended to the photocatalytic system at an industrial scale (considering 15–45 kg day^{-1} of nanocatalyst production and 10–30 m^3 of wastewater), which is discussed in the following section.

3.3. Economical analysis

Table 4 shows the costs involved in the investment in the wastewater plant, where the total cost for 15, 30, and 45 kg day^{-1} of nSOD@CuO-NPs is US$ 4239.15, US$ 6415.69, and US$ 8502.04, respectively. In addition, labor cost and additional costs (nanozeolite and nanocatalyst syntheses) accounted for US$ 778,500.00.

Table S4 informs the cost of investment associated with the acquisition of equipment and territory for wastewater plant implementation, where the investment cost for the wastewater plant implementation, including the pieces of equipment required to produce the nanocatalyst was estimated at US$ 530,367.99. Based on this, a cash flow analysis for the three production systems (15, 30, and 45 kg day^{-1}) was carried out, and the results are presented in Table S5.

According to Table S4, the total cost of investment for 15, 30, and 45 kg day^{-1} of nSOD@CuO-NPs was US$ 1,134,590.94, US$ 1,136,767.48, and US$ 1,138,853.83, respectively. These values include labor costs, purchase of the territory (land), and operation/chemical conversion units. Over a period of 1 to 10 years, the projected revenues (cash inflows) were estimated based on the annual costs for treating wastewater containing a binary mixture of dyes. These estimates consider the use of three production systems with daily nanocatalyst outputs of 15, 30, and 45 kg of nSOD@CuO-NPs, corresponding to treatment capacities of 10, 20, and 30 m^3 of wastewater, respectively. The evaluated cumulative revenues over the period amounted to approximately US$ 1,146,960.00, US$ 1,265,220.00, and US$ 1,383,480.00 for the respective systems.

It is important to highlight that the estimated cost of US$ 16.20 per unit for obtaining Al_2O_3 from alum sludge accounts only for the pretreatment steps (drying and calcination). This is because the untreated alum sludge was kindly provided free of charge through local partnerships within the project area. Therefore, the estimated cost of US$ 16.20 corresponds solely to the processing required to convert the alum sludge into a usable Al_2O_3 source.

Table S5 shows the economic analysis for the three production systems, in terms of NPV, IRR, B/C, and DPP.

Table 4
Raw material and labor costs information.

Raw material/equipment	Unit price (US$ kg^{-1})	Quantity required (kg)	Investment cost (US$)
Production of 15 kg day^{-1}			
Sodium hydroxide (NaOH)	209.65	2.12	444.25
Silicon dioxide (SiO_2)	50.00	2.97	148.50
Aluminum oxide (Al_2O_3) from alum sludge	–	9.48	16.20*
Green tea leaves (*Camellia sinensis*)	20.00	6.76	135.20
Copper (II) chloride dihydrate ($CuCl_2{\cdot}2H_2O$)	150.00	9.65	1447.50
Ammonium hydroxide (NH_4OH)	30.00	68.25	2047.50
Total cost			4239.15
Production of 30 kg day^{-1}			
Sodium hydroxide (NaOH)	209.65	4.24	888.29
Silicon dioxide (SiO_2)	50.00	5.94	297.00
Aluminum oxide (Al_2O_3) from alum sludge	–	18.95	16.20*
Green tea leaves (*Camellia sinensis*)	20.00	13.51	270.20
Copper (II) chloride dihydrate ($CuCl_2{\cdot}2H_2O$)	150.00	19.31	2896.50
Ammonium hydroxide (NH_4OH)	30.00	68.25	2047.50
Total cost			6415.69
Production of 45 kg day^{-1}			
Sodium hydroxide (NaOH)	209.65	6.36	1332.54
Silicon dioxide (SiO_2)	50.00	8.91	445.50
Aluminum oxide (Al_2O_3) from alum sludge	–	28.43	16.20*
Green tea leaves (*Camellia sinensis*)	20.00	20.27	405.40
Copper (II) chloride dihydrate ($CuCl_2{\cdot}2H_2O$)	150.00	28.96	4344.00
Ammonium hydroxide (NH_4OH)	30.00	65.25	1958.40
Total cost			8502.04
Additional costs: labor costs (workers) / (US$ year^{-1}) + additional costs			778,500.00

* Energetic cost associated with thermal treatment in industrial furnace (Capacity: 600 L | Power: 60 kW) at 400 °C for 4 h | Additional costs: hydrothermal synthesis of nSOD (180 °C, 6 h) and thermal treatment used in nSOD@CuO-NPs synthesis (450 °C, 4 h).

According to Table S5, all systems resulted in positive Net Present Value (NPV), Cost-Benefit ratio (B/C), and Internal Return Rate (IRR) greater than the interest rate ($i = 12$ %) used in this study. Moreover, shorter DPP values and IRR $> i$ suggest that a project is economically feasible [67]. Additionally, a B/C ratio greater than 1 indicates that the benefits exceed the costs, which is another indicator of project feasibility [68]. Thus, for the three proposed systems, the DPP ranged from 2 to 4 years, which are considerably short and positive in terms of economic analysis [69]. Therefore, these results suggest the reliability of all three production systems.

Furthermore, the system 1 (15 kg day^{-1} | wastewater treatment capacity of 10 m^3) exhibited NPV = 1,398,283.73, and IRR = 36.9 %. However, system 1 resulted in the least cost-benefit ratio (B/C = 1.23), characterizing it as the project with the lowest reliability.

In parallel, the system 2 (30 kg day^{-1} | wastewater treatment capacity of 20 m^3) an exhibited higher NPV (US$ 2,130,975.82), IRR (48.7 %) and C/B (1.87) and a DPP of 2 years, suggesting greater reliability than system 1.

Regarding system 3 (45 kg day^{-1} | wastewater treatment capacity of 30 m^3), it was reported a DPP of 2 years and a slightly higher NVP (US$ 2,845,471.11), IRR (59.7 %), and B/C (2.50) values than system 2. The highest IRR (significantly exceeding the interest rate, $i = 12$ %) e B/C values for system 3 revealed that this system was the most reliable project, as it generates the highest benefits relative to costs among the proposed systems, enabling a faster return on the initial investment [70].

4. Conclusion

In this study, it was allowed for an exploratory data analysis and economic feasibility analysis for the treatment of a binary dye mixture (crystal violet and methylene blue) using a heterogeneous photocatalysis process with a supported green nanocatalyst with a catalytic matrix of nSOD from aluminum sludge and rice husks waste and a photoactive phase of CuO-NPs from green tea (*Camellia sinensis*) extract. For this, an Exploratory Data Analysis (EDA) was performed using Spearman's correlation and data visualization to evaluate the effect of the photocatalytic parameters and reactor volume on the removal of the synthetic dyes CV and MB. The energy and operational costs of a laboratory-scale system were assessed to determine the total cost required to treat 1.0 L of wastewater containing the binary dye mixture. Additionally, an economic feasibility analysis was carried out for scaled-up systems with volumes of 10, 20, and 30 m^3, corresponding to nanocatalyst production capacities of 15 kg day^{-1} (system 1), 30 kg day^{-1} (system 2), and 45 kg day^{-1} (system 3). All three production systems were found economically viable over a 10-year period, yielding returns on initial investment of 36.9 %, 48.7 %, and 59.71 %, respectively. Furthermore, a DPP of 4 years was estimated for system 1, and 2 years for systems 2 and 3, with system 3 resulting in the highest cost-benefit ratio (2.50 dollars returned for every 1.00 dollar invested). Therefore, the proposed production system for green copper-based nanocatalysts was considered promising for treating wastewater contaminated with dyes, capable of processing volumes ranging from 10 to 30 m^3. This conclusion is supported by economic analysis and based on scale-up results from laboratory experiments, which demonstrated the degradation of approximately 92–95 % of a binary dye mixture within 4 h. In addition, the proposed photocatalysis system and photocatalyst proved to be economically viable for industrial applications, being able to mitigate the adverse environmental impacts generated by the textile industries and encourage the valorization of solid waste, correlating green nanotechnology and sustainable development. It is noteworthy that new perspectives will be evaluated for future work, such as policy interventions, techno-economic analysis (TEA), and life cycle analysis (LCA).

CRediT authorship contribution statement

Leandro Rodrigues Oviedo: Writing – review & editing, Writing – original draft, Validation, Investigation, Formal analysis, Data curation. **Sthéfany Nunes Loureiro:** Writing – review & editing, Writing – original draft, Methodology, Formal analysis, Data curation. **Lissandro Dorneles Dalla Nora:** Writing – review & editing, Validation, Supervision, Methodology, Formal analysis, Data curation. **William Leonardo da Silva:** Writing – review & editing, Writing – original draft, Validation, Supervision, Project administration, Investigation, Funding acquisition, Formal analysis, Data curation, Conceptualization.

Declaration of competing interest

The authors declare that they have no known competing financial interests or personal relationships that could have appeared to influence the work reported in this paper.

Acknowledgments

Authors would also like to thank Franciscan University for instrumental support. This study was financed by the CAPES (Coordination of Superior Level Staff Improvement) - Finance Code 001.

Appendix A. Supplementary data

Supplementary data to this article can be found online at https://doi.org/10.1016/j.jwpe.2025.108508.

Data availability

The data that support the findings of this study are available on request from the corresponding author.

References

[1] B. Pratap, S. Kumar, S. Nand, I. Azad, R.N. Bharagava, L.F. Romanholo Ferreira, V. Dutta, Wastewater generation and treatment by various eco-friendly technologies: possible health hazards and further reuse for environmental safety, Chemosphere 313 (2023) 137547–137559, https://doi.org/10.1016/j.chemosphere.2022.137547.

[2] N.V. Mdlovu, N.-C. Yang, K.-S. Lin, C.-J. Chang, K.T. Dinh, Y.-G. Lin, Formulation and characterization of W-doped titania nanotubes for adsorption/photodegradation of methylene blue and basic violet 3 dyes, Catal. Today 388 (2022) 36–46, https://doi.org/10.1016/j.cattod.2021.03.015.

[3] S. Mohanty, S. Moulick, S.K. Maji, Adsorption/photodegradation of crystal violet (basic dye) from aqueous solution by hydrothermally synthesized titanate nanotube (TNT), J. Water Process Eng. 37 (2020) 101428–101438, https://doi.org/10.1016/j.jwpe.2020.101428.

[4] J. Sharma, S. Sharma, V. Soni, Classification and impact of synthetic textile dyes on aquatic flora: a review, Reg. Stud. Mar. Sci. 45 (2021) 101802–101819, https://doi.org/10.1016/j.rsma.2021.101802.

[5] R. Al-Tohamy, S.S. Ali, F. Li, K.M. Okasha, Y.A.-G. Mahmoud, T. Elsamahy, H. Jiao, Y. Fu, J. Sun, A critical review on the treatment of dye-containing wastewater: Ecotoxicological and health concerns of textile dyes and possible remediation approaches for environmental safety, Ecotoxicol. Environ. Saf. 231 (2022) 113160–113177, https://doi.org/10.1016/j.ecoenv.2021.113160.

[6] N. Bux, S.H. Tumrani, R.A. Soomro, Q. Ma, J. Zhou, T. Wang, Catalytic degradation of organic pollutants in aqueous systems: a comprehensive review of peroxyacetic acid-based advanced oxidation processes, J. Environ. Manage. 373 (2025) 123989–124000, https://doi.org/10.1016/j.jenvman.2024.123989.

[7] S. Mohd, A.M. Khan, Heterogeneous photocatalysis: recent advances and applications, in: M. Sen (Ed.), Sustainable Green Catalytic Processes, 1st ed., Wiley, 2024, pp. 141–163, https://doi.org/10.1002/9781394212767.ch7.

[8] S. Pandey, P. Rawat, A. Ram, S.K. Chauhan, R.N. Singh, R.K. Shukla, A. Srivastava, The mechanistic pathway of paracetamol degradation using UV/H_2O_2 with PVP functionalized ZnO nanorods, J. Mol. Struct. 1317 (2024) 139068–139079, https://doi.org/10.1016/j.molstruc.2024.139068.

[9] D. Friedmann, A general overview of heterogeneous photocatalysis as a remediation technology for wastewaters containing pharmaceutical compounds, Water 14 (2022) 3588–3613, https://doi.org/10.3390/w14213588.

[10] K. Mubeen, A. Irshad, A. Safeen, U. Aziz, K. Safeen, T. Ghani, K. Khan, Z. Ali, I. Ul Haq, A. Shah, Band structure tuning of ZnO/CuO composites for enhanced photocatalytic activity, J. Saudi Chem. Soc. 27 (2023) 101639–101652, https://doi.org/10.1016/j.jscs.2023.101639.

[11] F. Soori, A. Nezamzadeh-Ejhieh, Synergistic effects of copper oxide-zeolite nanoparticles composite on photocatalytic degradation of 2,6-dimethylphenol aqueous solution, J. Mol. Liq. 255 (2018) 250–256, https://doi.org/10.1016/j.molliq.2018.01.169.

[12] I. Khaldari, M.R. Naghavi, E. Motamedi, Synthesis of green and pure copper oxide nanoparticles using two plant resources via solid-state route and their phytotoxicity assessment, RSC Adv. 11 (2021) 3346–3353, https://doi.org/10.1039/d0ra09924d.

[13] M. Yoldi, E.G. Fuentes-Ordoñez, S.A. Korili, A. Gil, Zeolite synthesis from industrial wastes, Microporous Mesoporous Mater. 287 (2019) 183–191, https://doi.org/10.1016/j.micromeso.2019.06.009.

[14] J. Fernández-Catalá, M. Sánchez-Rubio, M. Navlani-García, Á. Berenguer-Murcia, D. Cazorla-Amorós, Synthesis of TiO_2/nanozeolite composites for highly efficient photocatalytic oxidation of propene in the gas phase, ACS Omega 5 (2020) 31323–31331, https://doi.org/10.1021/acsomega.0c04793.

[15] A. Chakraborty, D.A. Islam, H. Acharya, Facile synthesis of CuO nanoparticles deposited zeolitic imidazolate frameworks (ZIF-8) for efficient photocatalytic dye degradation, J. Solid State Chem. 269 (2019) 566–574, https://doi.org/10.1016/j.jssc.2018.10.036.

[16] A. Nezamzadeh-Ejhieh, M. Karimi-Shamsabadi, Comparison of photocatalytic efficiency of supported CuO onto micro and nano particles of zeolite X in photodecolorization of methylene blue and methyl orange aqueous mixture, Appl. Catal. Gen. 477 (2014) 83–92, https://doi.org/10.1016/j.apcata.2014.02.031.

[17] L.R. Oviedo, D.M. Druzian, L.D.D. Nora, W.L. Da Silva, Biosynthesis and characterization of a novel supported nanocatalyst for the methylene blue dye photodegradation: machine learning modeling and photocatalytic activity, Catal. Today 441 (2024) 114888–114895, https://doi.org/10.1016/j.cattod.2024.114888.

[18] S. Sumitha, P.S. Jeba Sagana, E. Subramanian, K. Swarnalatha, Catalytic oxidative degradation of crystal violet dye using nanocopper oxide encapsulated zeolite catalyst, Results Surf. Interfaces 13 (2023) 100164–100173, https://doi.org/10.1016/j.rsurfi.2023.100164.

[19] I.J. Lithi, K.I.A. Nakib, A.M.S. Chowdhury, M.S. Hossain, A review on the green synthesis of metal (Ag, Cu, and Au) and metal oxide (ZnO, MgO, Co_3O_4, and TiO_2) nanoparticles using plant extracts for developing antimicrobial properties, Nanoscale Adv. 7 (2025) 2446–2473, https://doi.org/10.1039/d5na00037h.

[20] R.V. Bordiwala, Green synthesis and applications of metal nanoparticles.- a review article, Results Chem. 5 (2023) 100832–100835, https://doi.org/10.1016/j.rechem.2023.100832.

[21] M.D.C.R. da Silva, D.M. Druzian, L.F.W. Brum, C. dos Santos, G. Pavoski, D.C. R. Espinosa, Y.P.M. Ruiz, A. Galembeck, W.L. da Silva, Green synthesis of ZrO_2/PdO-NPs for photodegradation of anionic dyes: photocatalytic activity and machine learning modelling, J. Mol. Liq. 410 (2024) 125581–125599, https://doi.org/10.1016/j.molliq.2024.125581.

[22] A.L.M. Nunes, L.R. Oviedo, M.D.C.R. da Silva, C. dos Santos, G. Pavoski, D.C. R. Espinosa, W.L. da Silva, Machine learning-guided photocatalytic degradation of Eriochrome black T using green Nb_2O_5-NPs@CeO_2-NPs, Inorg. Chem. Commun. 179 (2025) 114779–114789, https://doi.org/10.1016/j.inoche.2025.114779.

[23] G. Yashni, A. Al-Gheethi, R.M.S. Radin Mohamed, N.V. Dai-Viet, A.A. Al-Kahtani, M. Al-Sahari, N.J. Nor Hazhar, E. Noman, S. Alkhadher, Bio-inspired ZnO NPs synthesized from ipeels extract for Congo red removal from textile wastewater via photocatalysis: optimization, mechanisms, techno-economic analysis, Chemosphere 281 (2021) 130661–130673, https://doi.org/10.1016/j.chemosphere.2021.130661.

[24] E.H. Khader, T.J. Mohammed, T.M. Albayati, N.M.C. Saady, S. Zendehboudi, Green nanocatalyst for the photocatalytic degradation of organic pollutants in petroleum refinery wastewater: synthesis, characterization, and optimization, J. Mol. Struct. 1304 (2024) 137688, https://doi.org/10.1016/j.molstruc.2024.137688.

[25] J.M. Navia-Mendoza, O.A.E. Filho, L.A. Zambrano-Intriago, N.R. Maddela, M.M.M. B. Duarte, L.S. Quiroz-Fernández, R.J. Baquerizo-Crespo, J.M. Rodríguez-Díaz, Advances in the application of nanocatalysts in photocatalytic processes for the treatment of food dyes: a review, Sustainability 13 (2021) 11676–11704, https://doi.org/10.3390/su132111676.

[26] H. Liang, Applying three financial analysis methods in investment: a comparative case study, Adv. Econ. Manag. Political Sci. 145 (2025) 14–20, https://doi.org/10.54254/2754-1169/2024.ld19017.

[27] G. Drozdowski, Net present value (NPV) as a reinforcement of the decision-making process in terms of investment selection, Mark. Infrastruct. (2022) 1–6, https://doi.org/10.32843/infrastruct66-7.

[28] G. Drozdowski, Economic calculus qua an instrument to support sustainable development under increasing risk, J. Risk Financ. Manag. 14 (2021) 15–27, https://doi.org/10.3390/jrfm14010015.

[29] E.C. Nwude, A review on the calculation of return on investment, Int. J. Adv. Appl. Sci. 3 (2016) 110–119, https://doi.org/10.21833/ijaas.2016.09.016.

[30] R.A. Miller, Uncertainty in capital budgeting: five particular safety-(or danger-) margins from the NPV formula, J. Applied Corp. Finance 34 (2022) 110–115, https://doi.org/10.1111/jacf.12522.

[31] N.J.C. Neto, H.S. Ferreira, A.O. Nogueira, P.R.P. Freire, Methods for investment analysis: theoritcal and pratical presentation, J. Multidiscip. Res. 1 (2024) 1–9, https://doi.org/10.51473/rcmos.v1i1.2021.699.

[32] N. Saeidi, L. Lotteraner, G. Sigmund, T. Hofmann, M. Krauss, K. Mackenzie, A. Georgi, Towards a better understanding of sorption of persistent and mobile contaminants to activated carbon: applying data analysis techniques with experimental datasets of limited size, Water Res. 274 (2025) 123032–123041, https://doi.org/10.1016/j.watres.2024.123032.

[33] M. Shahid, S. Khalid, Z.A. ALothman, A.A. Al-Kahtani, I. Bibi, R. Naz, N. Natasha, N.K. Niazi, J. Iqbal, C. Han, N.S. Shah, B. Murtaza, Trace element removal from wastewater by agricultural biowastes: a data analysis on removal efficacy and optimized conditions, Sci. Total Environ. 975 (2025) 179235–179245, https://doi.org/10.1016/j.scitotenv.2025.179235.

[34] N.D. Abhinav, M. Sevanthi, S.Y.G. Yashaswini, Exploratory data analysis (EDA) and data visualization, Int. J. Innov. Res. Electr. Electron. Instrum. Control Eng. 12 (2024) 1–4, https://doi.org/10.17148/ijireeice.2024.12608.

[35] S. Dhummad, The imperative of exploratory data analysis in machine learning, Sch. J. Eng. Tech. 13 (2025) 30–44, https://doi.org/10.36347/sjet.2025.v13i01.005.

[36] L.R. Oviedo, D.M. Druzian, G.E. Montagner, Y.P.M. Ruiz, A. Galembeck, G. Pavoski, D.C.R. Espinosa, L.D. Dalla Nora, W.L. Da Silva, Supported heterogeneous catalyst of the copper oxide nanoparticles and nanozeolite for binary dyes mixture degradation: machine learning and experimental design, J. Mol. Liq. 402 (2024) 124763–124781, https://doi.org/10.1016/j.molliq.2024.124763.

[37] S. Tabassum, Md. Sahadat Hossain, D. Islam, S. Ahmed, Synthesis of nano-crystallite β-Bi_2O_3 as a photocatalyst through solid-state method for a sturdy treatment of pharmaceutical waste, Results Surf. Interfaces 18 (2025) 100371–100384, https://doi.org/10.1016/j.rsurfi.2024.100371.

[38] R.H.A. Murti, M.A.S. Jawwad, K.K. Ayuningtiyas, E.N. Hidayah, High efficiency on resin photocatalysis: study on application and kinetic mechanism using Langmuir-hinshelwood model, S. Afr. J. Chem. Eng. 53 (2025) 87–95, https://doi.org/10.1016/j.sajce.2025.04.013.

[39] L. Leng, L. Yang, X. Lei, W. Zhang, Z. Ai, Z. Yang, H. Zhan, J. Yang, X. Yuan, H. Peng, H. Li, Machine learning predicting and engineering the yield, N content, and specific surface area of biochar derived from pyrolysis of biomass, Biochar 4 (2022) 63–81, https://doi.org/10.1007/s42773-022-00183-w.

[40] D.A. Yaseen, M. Scholz, Textile dye wastewater characteristics and constituents of synthetic effluents: a critical review, Int. J. Environ. Sci. Technol. 16 (2019) 1193–1226, https://doi.org/10.1007/s13762-018-2130-z.
[41] D.J. Brennan, K.A. Golonka, New factors for capital cost estimation in evolving process designs, Chem. Eng. Res. Des. 80 (2002) 579–586, https://doi.org/10.1205/026387602760312773.
[42] R. Barbosa, B. Escobar, V.M. Sánchez, J. Ortegón, Effects of the size and cost reduction on a discounted payback period and levelized cost of energy of a zero-export photovoltaic system with green hydrogen storage, Heliyon 9 (2023), https://doi.org/10.1016/j.heliyon.2023.e16707 e16707-e16721.
[43] A. Biswas, S. Chakraborty, Cost benefit analysis of integrated constructed wetland microbial fuel cell system for sustainable and economic domestic wastewater treatment, Sustain. Energy Technol. Assess. 60 (2023) 103475–103484, https://doi.org/10.1016/j.seta.2023.103475.
[44] V.R. Oviedo, D.M. Druzian, S.R. Mortari, M.R. Sagrillo, T.M. Volkmer, D.A. Bertuol, L.F. Rodrigues Jr., Synthesis and characterization of SrO-containing bioglass-ceramic from rice husk silicon dioxide, Cerâmica 66 (2020) 426–432, https://doi.org/10.1590/0366-69132020663802979.
[45] R. Turton, J.A. Shaeiwitz, D. Bhattacharyya, W.B. Whiting, Analysis, Synthesis, and Design of Chemical Processes, Fifth edition, Pearson Education Inc., New York, 2018.
[46] A. Fernández-Pérez, T. Valdés-Solís, G. Marbán, Visible light spectroscopic analysis of methylene blue in water; the resonance virtual equilibrium hypothesis, Dyes Pigments 161 (2019) 448–456, https://doi.org/10.1016/j.dyepig.2018.09.083.
[47] S.K. Eden, C. Li, B.E. Shepherd, Nonparametric estimation of Spearman's rank correlation with bivariate survival data, Biometrics 78 (2022) 421–434, https://doi.org/10.1111/biom.13453.
[48] Y.P. Moreno, W.L. Da Silva, F.C. Stedile, C. Radtke, J.H.Z. Dos Santos, Micro and nanodomains on structured silica/titania photocatalysts surface evaluated in RhB degradation: effect of structural properties on catalytic efficiency, Appl. Surf. Sci. 3 (2021) 100055–100069, https://doi.org/10.1016/j.apsadv.2021.100055.
[49] J. Gomes, M. Roccamante, S. Cantreras, F. Medina, I. Oller, R.C. Martins, Scale-up impact over solar photocatalytic ozonation with benchmark-P25 and N-TiO2 for insecticides abatement in water, J. Environ. Chem. Eng. 9 (2021) 103915–103929, https://doi.org/10.1016/j.jece.2020.104915.
[50] J.B. Fathima, A. Pugazhendhi, M. Oves, R. Venis, Synthesis of eco-friendly copper nanoparticles for augmentation of catalytic degradation of organic dyes, J. Mol. Liq. 260 (2018) 1–8, https://doi.org/10.1016/j.molliq.2018.03.033.
[51] U.K. Saint, S.C. Baral, D. Sasmal, P. Maneesha, S. Datta, F. Naushin, S. Sen, Effect of pH on photocatalytic degradation of methylene blue in water by facile hydrothermally grown TiO2 nanoparticles under natural sunlight, Mater. Sci. 2025 (2024) 1–33, https://doi.org/10.48550/arXiv.2411.08515.
[52] A.A. Al-Massaedh, F.I. Khalili, A. Al Shra'ah, Adsorptive removal of cationic dyes (methylene blue and crystal violet) from aqueous solutions using anionic polyacrylamide-based monolith, Desalin. Water Treat. 270 (2022) 260–274, https://doi.org/10.5004/dwt.2022.28780.
[53] S. David, S. Kim, S. Oh, Y.H. Kahng, Advances in decorated mobile composites for adsorption and photocatalytic dye degradation: a comprehensive review, J. Hazard. Mater. Adv. 18 (2025) 100600–100626, https://doi.org/10.1016/j.hazadv.2025.100600.
[54] M. Ghavami, R. Mohammadi, M. Koohi, M.Z. Kassaee, Visible light photocatalytic activity of reduced graphene oxide synergistically enhanced by successive inclusion of γ-Fe_2O_3, TiO_2, and Ag nanoparticles, Mater. Sci. Semicond. 26 (2014) 69–78, https://doi.org/10.1016/j.mssp.2014.04.007.
[55] D.K. Bhatt, U.D. Patel, Photocatalytic degradation of reactive black 5 using Ag_3PO_4 under visible light, J. Phys. Chem. Solids 149 (2021) 109768–109778, https://doi.org/10.1016/j.jpcs.2020.109768.
[56] D.M. Druzian, L.R. Oviedo, R.D. Wouters, S.N. Loureiro, Y.P.M. Ruiz, A. Galembeck, G. Pavoski, D.C.R. Espinosa, C. Dos Santos, J.H.Z. Dos Santos, W.L. D. Silva, A bimetallic nanocatalyst from carbonaceous waste for crystal violet degradation, Mater. Chem. Phys. 297 (2023) 127455–127465, https://doi.org/10.1016/j.matchemphys.2023.127455.
[57] A.I. Licona–Aguilar, A.M. Torres–Huerta, M.A. Domínguez–Crespo, M.L. X. Negrete–Rodríguez, E. Conde–Barajas, S.B. Brachetti–Sibaja, A. E. Rodríguez–Salazar, Valorization of agroindustrial orange peel waste during the optimization of activated carbon–multiwalled carbon nanotubes–zinc oxide composites used in the removal of methylene blue in wastewater, Chem. Eng. J. 492 (2024) 152102–152115, https://doi.org/10.1016/j.cej.2024.152102.
[58] S. Shoukat, H.N. Bhatti, M. Iqbal, S. Noreen, Mango stone biocomposite preparation and application for crystal violet adsorption: a mechanistic study, Microporous Mesoporous Mater. 239 (2017) 180–189, https://doi.org/10.1016/j.micromeso.2016.10.004.
[59] S. Ouni, F. Yahia, N. BelHaj Mohamed, M. Bouzidi, A.S. Alshammari, F. Abdulaziz, A. Bonilla-Petriciolet, M. Mohamed, Z.R. Khan, N. Chaaben, M. Haouari, Effective removal of textile dye via synergy of adsorption and photocatalysis over ZnS nanoparticles: synthesis, modeling, and mechanism, Heliyon 10 (2024), https://doi.org/10.1016/j.heliyon.2024.e36949 e36949–e36968.
[60] H. Lazarova, R. Rusew, K. Iliev, L. Tsvetanova, B. Barbov, B. Shivachev, Photodegradation of methylene blue and crystal violet by Zr-modified Engelhard titanium silicate 10, Water 15 (2023) 4186–4204, https://doi.org/10.3390/w15234186.
[61] K. Patel, T. Parangi, G.K. Solanki, M.K. Mishra, K.D. Patel, V.M. Pathak, Photocatalytic degradation of methylene blue and crystal violet dyes under UV light irradiation by sonochemically synthesized CuSnSe nanocrystals, Eur. Phys. J. Plus 136 (2021) 743–760, https://doi.org/10.1140/epjp/s13360-021-01725-0.
[62] J.M. Navia-Mendoza, O.A.E. Filho, L.A. Zambrano-Intriago, N.R. Maddela, M.M.M. B. Duarte, L.S. Quiroz-Fernández, R.J. Baquerizo-Crespo, J.M. Rodríguez-Díaz, Advances in the application of nanocatalysts in photocatalytic processes for the treatment of food dyes: a review, Sustainability 13 (2021) 11676–11695, https://doi.org/10.3390/su132111676.
[63] H. Mirhosseini, T. Shamspur, A. Mostafavi, Novel adsorbent g-C_3N_4/ZnV_2O_4 for efficient removal of crystal violet dye: removal process optimization, adsorption isotherms, and kinetic modeling, Appl. Organomet. Chem. 36 (2022) e6867–e6879, https://doi.org/10.1002/aoc.6867.
[64] S. Janitabar Darzi, Dye sensitization pathway in the visible light photodegradation of crystal violet on TiO_2 surface, Mater. Chem. Mech. 1 (2023) 30–38, https://doi.org/10.22034/mcm.2023.1.3.
[65] M.M. Sajid, S.B. Khan, N.A. Shad, N. Amin, Z. Zhang, Visible light assisted photocatalytic degradation of crystal violet dye and electrochemical detection of ascorbic acid using a $BiVO_4$/$FeVO_4$ heterojunction composite, RSC Adv. 8 (2018) 23489–23498, https://doi.org/10.1039/c8ra03890b.
[66] M. Mittal, M. Sharma, O.P. Pandey, UV–visible light induced photocatalytic studies of Cu doped ZnO nanoparticles prepared by co-precipitation method, Sol. Energy 110 (2014) 386–397, https://doi.org/10.1016/j.solener.2014.09.026.
[67] A.H. Alshami, H.A. Hussein, Feasibility analysis of mini hydropower and thermal power plants at Hindiya barrage in Iraq, Ain Shams Eng. J. 12 (2021) 1513–1521, https://doi.org/10.1016/j.asej.2020.08.034.
[68] D.A. Mellichamp, Internal rate of return: good and bad features, and a new way of interpreting the historic measure, Comput. Chem. Eng. 106 (2017) 396–406, https://doi.org/10.1016/j.compchemeng.2017.06.005.
[69] C.A. Magni, Average internal rate of return and investment decisions: a new perspective, Eng. Econ. 55 (2010) 150–180, https://doi.org/10.1080/00137911003791856.
[70] O.E. Umeagukwu, D.O. Onukwuli, C.N. Ude, C. Esonye, B.N. Ekwueme, C. O. Asadu, F.C. Okey-Onyesolu, M.U. Ikenna, E.I. Chukwudi, T. Makhkamov, S. Islamov, I.M. Yormukhamatovna, Transesterification of *Persea americana* seed oil to methyl ester using bio-based heterogeneous catalyst: optimization and techno-economic analysis, Green Technologies and Sustainability 2 (2024) 100086–100105, https://doi.org/10.1016/j.grets.2024.100086.